Nonlinear normal modes of a two degrees-of-freedom piecewise linear system

El Hadi Moussi, Sergio Bellizzi, Bruno Cochelin, Ionel Nistor

Nonlinear normal modes of a two degrees-of-freedom piecewise linear system

E.H. Moussi [a,b], S. Bellizzi [a], B. Cochelin [a], I. Nistor [b]

[a] LMA, CNRS, UPR 7051, Centrale Marseille, Aix-Marseille Univ, F-13402 Marseille Cedex 20, France
[b] LaMSID, UMR EDF-CNRS-CEA 2832, 1 Avenue du Général de Gaulle, 92141 Clamart, France

A study of the Nonlinear Normal Modes (NNMs) of a two degrees of freedom mechanical system with a bilateral elastic stop for one of them is considered. The issue related to the non-smoothness of the impact force is handled through a regularization technique. The Harmonic Balance Method (HBM) with a large number of harmonics, combined with the Asymptotic Numerical Method (ANM), is used to solve the regularized problem. The results are validated from periodic orbits obtained analytically in the time domain by direct integration of the non-regular problem. The first NNM shows an elaborate dynamics with the occurrence of multiple impacts per period, internal resonance and instabilities. On the other hand, the second NNM presents a more simple, almost linear, dynamics. The two NNMs converge asymptotically (for an infinite energy) toward two other Linear Normal Modes, corresponding to the system with a gap equal to zero.

Keywords:
Nonlinear normal mode
Piecewise linear system
Periodic orbit
Stability
Harmonic balance method
Asymptotic numerical method

1. Introduction and industrial issue

Many engineering systems involve components with clearance and intermittent contact. This type of nonlinearities is relevant for example in nuclear power plants, specifically in steam generator. In vibration analysis this type of nonlinearities can be modeled considering piecewise linear elastic stops [29,8] or nonlinear elastic stops [7] or rigid impacts [16]. Such nonsmooth systems have been subject of numerous investigations specially to analyze forced responses. The following references [31,35,1,9] give a small selection of the developed procedures.

Recent works have shown that the Nonlinear Normal Modes (NNMs) constitute an efficient vibration analysis framework for nonlinear mechanical systems from theoretical [34,15] as well as experimental [24] point of view. The NNMs can be viewed as an extension of the concept of the normal modes in the theory of the linear systems to nonlinear ones. One of the most attractive definitions is due to Shaw and Pierre [30] in terms of a two-dimensional invariant manifold in phase space. This definition has the advantage that it is valid for conservative and non-conservative systems. However in case of conservative systems, a more numerically tractable definition can be used. This definition is an extension of the definition introduced by Rosenberg [27] and considers a NNM as a family of free motion parametrized by energy level. Hence, the

NNMs can be computed using numerical continuation techniques of periodic solutions in conservative system. An approach combining a shooting method to approximate the periodic orbit in time domain and the pseudo-arclength continuation method is proposed in [25] to compute the NNMs. Another methodology combining the Harmonic Balance Method (HBM) to approximate the periodic orbit and the Asymptotic Numerical Method (ANM) [4] as a continuation method is discussed in [6,14] to compute the periodic solutions of dynamical systems and can be advantageously used to compute the NNMs. The first step of this methodology is to recast the dynamical system in quadratic polynomial form before applying the HBM resulting in optimal form to apply the ANM method. In [6], polynomial nonlinearities are considered whereas in [14] the procedure is extended to non-polynomial nonlinearities. Other approaches exist like combining the alternating frequency/ time-domain harmonic balance method (AFT-HBM) with the pseudo-arclength continuation method to compute mostly forced response [12,9]. Note that in the last two references, the selection procedures of the number of harmonics in the HBM procedure are proposed and investigated.

The concept of NNMs is not limited to smooth systems. Nonsmooth systems have received great attention in regard to NNMs. Conservative piecewise linear vibratory systems were considered in [3,13] where NNMs were obtained using the invariant manifolds form. In [21] the concept of NNMs formulated as a functional relation between the two coordinates of the system was used to analyze a two Degrees Of Freedom (DOF) system with vibro-impact allowing the computation of various branches of bifurcating periodic solutions with different impacting characteristics. Rigid elastic stops were considered in [33] where the NNMs of a single DOF linear system with a vibro-impact attachment were obtained by employing the method of nonsmooth transformation introduced in [26] to approximate the periodic orbit in time domain. In [23], the family of periodic solutions were found in analytical form for a conservative two DOF oscillator with elastic and rigid stop. In [17], a dissipative system is considered and a Fourier series including decreasing exponential terms is used to approximate the NNMs combined with a HBM formulation.

Though many researchers have examined the problem of computing the nonlinear normal modes for nonsmooth systems, few tools to analyze the complete behavior of the NNMs including bifurcation diagram analysis, internal resonances characterization and stability properties are available. In this context, the objective of this paper is to demonstrate that a method combining the HBM method (to approximate the periodic responses) and the ANM (to carry out the continuation of branches of periodic orbits) to analyze the NNMs of a nonsmooth system can be efficient. As suggested in [6], the efficiency of the HBM and ANM will be ensured introducing a regularization of the nonsmooth terms using a family of implicit polynomial. A two degrees of freedom oscillator with a bilateral elastic stop have been used to carry out the study. It is an analogy with a simplified model of the out-of-plane bending of U-tube going through supporting plates as shown in Fig. 1. Similar two degrees-of-freedom systems have been considered in [3,13,23].

The paper is organized as follows. In the next section, the nonsmooth model under consideration is described and periodic orbits with two impacts per period are investigated. Section 3 is dedicated to the description of the proposed procedure to compute the NNM branches. A regularized model is first introduced and the HBM and ANM methods are next described. Finally, in Section 4, the results for the NNMs are discussed in detail, analyzing the influence of the regularization parameters.

2. Nonsmooth model under consideration

2.1. A two degrees of freedom oscillator with an elastic stop

The system under consideration is shown Fig. 1 (right side). It consists of two masses m_1 and m_2 connected by two linear springs of stiffness k_1 and k_2. The motion of the mass m_1 is limited by a bilinear elastic stop with a linear spring of stiffness K

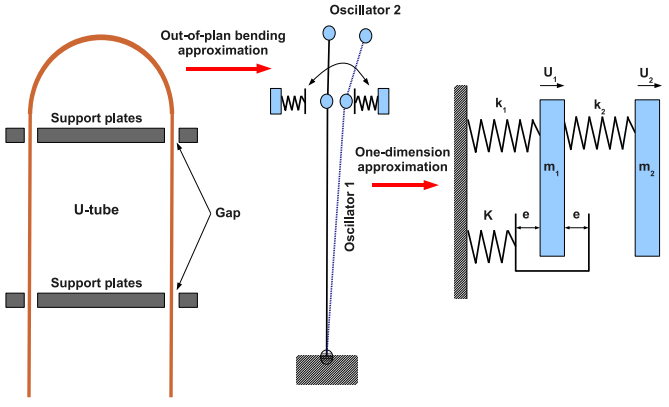

Fig. 1. Analogy of a simplified model of a U-tube with a two degrees of freedom oscillator.

and a gap e. The equations of motion are given by

$$\begin{cases} m_1\ddot{U}_1(t)+k_1U_1(t)+k_2(U_1(t)-U_2(t))+F(U_1(t))=0 \\ m_2\ddot{U}_2(t)+k_2(U_2(t)-U_1(t))=0 \end{cases} \tag{1}$$

with

$$F(U)=\begin{cases} K(U-e) & \text{if } e\le U \\ 0 & \text{if } -e\le U\le e \\ K(U+e) & \text{if } U\le -e \end{cases} \tag{2}$$

where U_i denotes the displacement of the mass m_i (for $i=1,2$) and F denotes the bilateral contact force. Using now the following rescaled quantities $x=U_1/e$, $u=U_2/e$, $\hat{f}=F/k_1e$ and the time normalization $\tau=\omega t$ with $\omega=\sqrt{k_1/m_1}$, Eqs. (1) and (2) take the following nondimensional form:

$$\begin{cases} \ddot{x}(\tau)+x(\tau)+\beta(x(\tau)-u(\tau))+\hat{f}(x(\tau))=0 \\ \delta\ddot{u}(\tau)+\beta(u(\tau)-x(\tau))=0 \end{cases} \tag{3}$$

with

$$\hat{f}(x)=\begin{cases} \alpha(x-1) & \text{if } 1\le x \\ 0 & \text{if } -1\le x\le 1 \\ \alpha(x+1) & \text{if } x\le -1 \end{cases} \tag{4}$$

where $\beta=k_2/k_1$, $\alpha=K/k_1$, $\delta=m_2/m_1$ and $(\cdot)$ denotes now the time derivative with respect to the new time τ.

Eqs. (3) and (4) only depend on three parameters. The two parameters β and δ characterize the linear system and α characterizes the stop. In practice, α must be chosen large for a good representation of the stops. The gap parameter e is reduced to one in the nondimensional model. In the sequel, we will restrict the discussion to the piecewise linear system of Eqs. (3) and (4).

2.2. Computation of some periodic orbits

Based on the piecewise linear structure of Eqs. (3) and (4), it is possible to characterize some periodic solutions using event-driven resolution as in [23], or using other methods as in [21,31]. We focus on the synchronous oscillations (i.e. periodic vibration in unison: all material points of the system reach their extreme values and pass through zero simultaneously) which corresponds to the definition of the NNM proposed by Rosenberg [27]. Periodic orbits with two impacts per period (one impact per stop) can easily be obtained.

Starting from the equilibrium point $(x_0,u_0)=(0,0)$, a modal line in the configuration space can be decomposed in four branches (see Fig. 2):

- for $0\le\tau\le T_1$ where T_1 corresponds to $\dot{x}(T_1)=0$, $\dot{u}(T_1)=0$ with the associated extreme values $x(T_1)=\max_{0\le\tau\le T_1}x(\tau)$ with $x(T_1)>1$ and $u(T_1)=\max_{0\le\tau\le T_1}u(\tau)$;
- for $T_1<\tau\le T_2$ where T_2 corresponds to $x(T_2)=0$ and $u(T_2)=0$;
- for $T_2<\tau\le T_3$ where T_3 corresponds to $\dot{x}(T_3)=0$, $\dot{u}(T_3)=0$ with the associated extreme values $x(T_3)=\min_{T_2\le\tau\le T_3}x(\tau)$ with $x(T_3)<-1$ and $u(T_3)=\min_{T_2\le\tau\le T_3}u(\tau)$;
- for $T_3<\tau\le T_4$ where T_4 corresponds to $x(T_4)=0$ and $u(T_4)=0$.

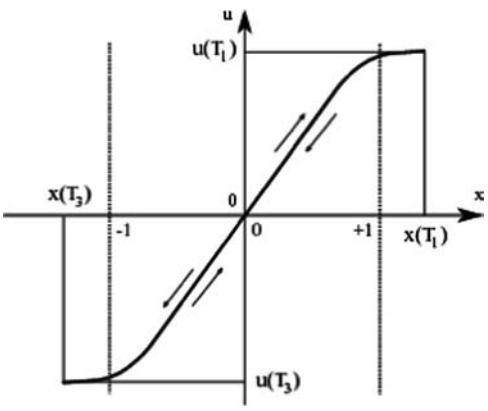

Fig. 2. Modal line with two impacts per period.

Due to the symmetry of the system, the branches satisfy the following relations:

- for $T_1 \le \tau \le T_2$, $x(t) = x(2T_1 - \tau)$ and $u(t) = x(2T_1 - \tau)$;
- for $T_2 \le \tau \le T_3$, $x(t) = -x(T_2 + T_1 - \tau)$ and $u(t) = x(T_2 + T_1 - \tau)$;
- for $T_3 \le \tau \le T_4$, $x(\tau) = -x(T_3 + T_1 - \tau)$ and $u(\tau) = x(T_3 + T_1 - \tau)$

showing that $T_2 = 2T_1$, $T_3 = 3T_1$ and $T_4 = 4T_1$. Hence, the period is equal to $T = T_4 = 4T_1$ and the periodic orbit is only characterized by the first branch (i.e. only on a quarter period).

Re-writing Eqs. (3) and (4) as

- for $-1 \le x(\tau) \le 1$,

$$\begin{cases} \ddot{x}(\tau) + x(\tau) + \beta(x(\tau) - u(\tau)) = 0 \\ \delta\ddot{u}(\tau) + \beta(u(\tau) - x(\tau)) = 0 \end{cases} \tag{5}$$

- for $x(\tau) \ge 1$,

$$\begin{cases} \ddot{x}(\tau) + (1+\alpha)x(\tau) + \beta(x(\tau) - u(\tau)) = \alpha \\ \delta\ddot{u}(\tau) + \beta(u(\tau) - x(\tau)) = 0 \end{cases} \tag{6}$$

- for $x(\tau) \le -1$,

$$\begin{cases} \ddot{x}(\tau) + (1+\alpha)x(\tau) + \beta(x(\tau) - u(\tau)) = -\alpha \\ \delta\ddot{u}(\tau) + \beta(u(\tau) - x(\tau)) = 0 \end{cases} \tag{7}$$

the first branch is defined in two steps:

- for $0 \le \tau \le \tau_1$, the branch solves the equations of motion (5) with the initial conditions $(0, 0, \dot{x}_0, \dot{u}_0)$ and the time duration τ_1 satisfies $x(\tau_1) = 1$;
- for $\tau_1 \le \tau \le T_1$, the branch solves the equations of motion (6) with the initial conditions $(1, 0, \dot{x}(\tau_1), \dot{u}(\tau_1))$ and the final time T_1 satisfies $\dot{x}(T_1) = 0$, $\dot{u}(T_1) = 0$.

Four unknowns $(\dot{x}_0, \dot{u}_0, \tau_1, T_1)$ are needed to characterize the quarter period branch and the unknowns satisfy three equations: $x(\tau_1) = 1$, $\dot{x}(T_1) = 0$, $\dot{u}(T_1) = 0$. As in [23], analytic expressions of the Cauchy problems associated to Eqs. (5) and (6) can be obtained. The expressions are not reported here for the sake of brevity. The resulting equations can be re-written in terms of a nonlinear algebraic system. This nonlinear algebraic system has been solved using the continuation Asymptotic Numerical Method (ANM) [4].

This approach gives access to the periodic orbits with two impacts per period of the two degrees of freedom oscillator with an elastic stop. It will be used to validate the method based on the HBM combined with a regularization of the nonsmooth terms using a family of implicit polynomial method which permits to compute more complicated dynamics.

3. Computation of the NNMs by HBM–ANM method

For autonomous conservative systems, a NNM may be defined as a family of periodic orbits as retained in [32,2,15]. To compute them, we develop a method combining (as done in [6,14]) the HBM method to approximate the NNM motions and the ANM method to give access to the branches of solution. The numerical efficiency of method proposed in [6] is here improved by using a different order of truncature on the Fourier series representation of unknown which permits a significant reduction of the dimension of the final algebraic system to be solved. For instance, a much higher order of truncature will be used for the impact force than for the displacement of the masses. Another point is that the method in [6] needs a regularization of the nonsmooth terms and this is done hereafter by using a family of implicit polynomial.

3.1. The associated two degrees of freedom oscillator with regularized elastic stop

Regularized equations of motion can be derived approximating the piecewise linear function (4) by the following implicit polynomial of degree three (with respect to the variable f)

$$f(f - \alpha(x-1))(f - \alpha(x+1)) + \eta\alpha^2 x = 0 \tag{8}$$

where η denotes the regularization parameter. We will assume in the sequel that $\eta \ge 0$. For $\eta = 0$, the possible values of $\hat{f}(x)$ for any given x (see (4)) appear to be the roots of the polynomial equation (8). For $\eta \ne 0$ and a given set of parameter values (x, α, η), the polynomial equation (8) always admits a real root denoted $f(x; \alpha, \eta)$ (the expression is not given here)

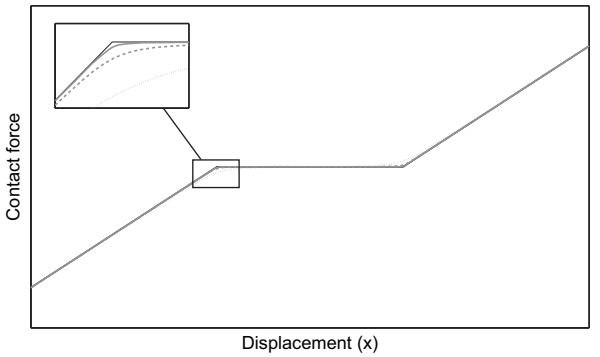

Fig. 3. Comparison of the piecewise-linear contact force obtained with Eq. (2) (in black) and the regularized contact force obtained with Eq. (9) (in grey) for different values of η. Parameter values: $\alpha=30$, $\eta=0.005$ (solid line), $\eta=0.05$ (dashed line), $\eta=0.5$ (dotted line).

represented in Fig. 3, which satisfies the following properties:

$$\begin{aligned} &\text{(i)} \quad x \text{ and } f(x;\alpha,\eta) \text{ have the same sign,}\\ &\text{(ii)} \quad f(x;\alpha,\eta) = -f(-x;\alpha,\eta),\\ &\text{(iii)} \quad \text{if } |x| \ll 1,\ f(x;\alpha,\eta) \approx \eta x,\\ &\text{(iv)} \quad \text{if } |x| \gg 1,\ f(x;\alpha,\eta) \approx \alpha(x+\text{sign}(x)). \end{aligned} \tag{9}$$

Hence, the regularized elastic stop can be viewed as an odd restoring force where the regularization parameter introduces a linear spring with stiffness coefficient η at the neighborhood of the equilibrium point $x=0$ (see Eq. (9)(iii)) and for large x reproduces the elastic stop behavior (see Eq. (9)(iv)). Finally, the regularized equations of motion defined by

$$\begin{cases} \ddot{x}(\tau)+x(\tau)+\beta(x(\tau)-u(\tau))+f(x(\tau);\alpha,\eta)=0 \\ \delta\ddot{u}(\tau)+\beta(u(\tau)-x(\tau))=0 \end{cases} \tag{10}$$

can advantageously replace Eqs. (3) and (4) when η is small compared to spring stiffness of the underlying linear system.

By introducing $z=(f/\alpha-x)^2$ as a new variable, Eq. (8) can be re-written in the quadratic form as

$$f-\eta x-fz=0 \tag{11}$$

and combining with Eq. (10), we obtain the following quadratic algebro-differential system:

$$\ddot{x}(\tau)+x(\tau)+\beta(x(\tau)-u(\tau))+f(\tau)=0 \tag{12}$$

$$\delta\ddot{u}(\tau)+\beta(u(\tau)-x(\tau))=0 \tag{13}$$

$$f(\tau)-\eta x(\tau)-f(\tau)z(\tau)=0 \tag{14}$$

$$z(\tau)-\left(\frac{f(\tau)}{\alpha}-x(\tau)\right)^2=0 \tag{15}$$

3.2. Computation of the branches of periodic orbits

The objective of this section is to develop a numerical tool which is able to compute the NNMs of the autonomous conservative system (10). The methodology combines the HBM and ANM approaches as described in [6,14] to compute the branches of periodic orbits. The main steps are described here after.

3.2.1. HBM step

The system (12)–(15) is first perturbed to obtain a quadratic algebro-differential system in a standard continuation framework to compute a family of periodic solutions (see [2,14]). To do this, damping terms are added to the first two equations (12) and (13) giving

$$\ddot{x}(\tau)+\lambda\dot{x}(\tau)+x(\tau)+\beta(x(\tau)-u(\tau))+f(\tau)=0 \tag{16}$$

$$\delta\ddot{u}(\tau)+\lambda\dot{u}(\tau)+\beta(u(\tau)-x(\tau))=0 \tag{17}$$

where λ is a free parameter.

The initial system (12)–(15) is then embedded into a general dissipative system (14)–(17) which possesses periodic solutions that are exactly those of the initial system if and only if $\lambda=0$. This way, the additional parameter λ defines an explicit control parameter to the continuation method.

Since the differential system is autonomous, a phase condition has to be added to define a unique periodic orbit [28,22]. Usually [2], this is done imposing a velocity degree of freedom, for example,

$$\dot{u}(0)=0 \tag{18}$$

The HBM method is now applied to the system (14)–(18).

The periodic orbit is approximated by a truncated Fourier series up to Hth term for the displacement variables u and x:

$$\begin{aligned} u(\tau) &= u_0+\sum_{k=1}^{H} u_c^k\cos(k\omega\tau)+u_s^k\sin(k\omega\tau) \\ x(\tau) &= x_0+\sum_{k=1}^{H} x_c^k\cos(k\omega\tau)+x_s^k\sin(k\omega\tau) \end{aligned} \tag{19}$$

and up to H_fth term for the nonlinear force f and the associated internal variable z:

$$\begin{aligned} f(\tau) &= f_0+\sum_{k=1}^{H_\mathrm{f}} f_c^k\cos(k\omega\tau)+f_s^k\sin(k\omega\tau) \\ z(\tau) &= z_0+\sum_{k=1}^{H_\mathrm{f}} z_c^k\cos(k\omega\tau)+z_s^k\sin(k\omega\tau) \end{aligned} \tag{20}$$

where as classical ω denotes the (unknown) frequency (which is related to the period as $T=2\pi/\omega$)). This formulation permits selecting $H_\mathrm{f}\gg H$ to improve the approximation of the nonlinear term. Indeed, $f(\tau)$ is almost zero when there is no contact and reach high values during contact. Then, its Fourier series representation requires more harmonics than for u and x.

Substituting Eqs. (19) and (20) and their second time derives into Eqs. (14)–(18) and balancing the terms of same frequency up to Hth term in Eqs. (16) and (17) and up to H_f th term in Eqs. (14) and (15), one obtains a nonlinear algebraic system of $2(2H+1)+2(2H_\mathrm{f}+1)+1$ equations which can be recasted, introducing the new variables $\gamma_1=\omega^2$ and $\gamma_2=\lambda\omega$, into a quadratic algebraic system of $2(2H+1)+2(2H_\mathrm{f}+1)+3$ as

$$\mathbf{R}(\mathbf{U}=\mathbf{L}(\mathbf{U})+\mathbf{Q}(\mathbf{U},\mathbf{U})=0 \tag{21}$$

where $\mathbf{U}=(\mathbf{U}_\mathrm{d}^T,\mathbf{U}_\mathrm{f}^T,\gamma_1,\gamma_2,\lambda,\omega)^T$ denotes the $2(2H+1)+2(2H_\mathrm{f}+1)+4$ unknown coefficients with

$$\mathbf{U}_\mathrm{d}=(u_0,x_0,u_c^1,x_c^1,u_s^1,x_s^1,\ldots,u_c^H,x_c^H,u_s^H,x_s^H)^T \tag{22}$$

$$\mathbf{U}_\mathrm{f}=(f_0,f_c^1,f_s^1,\ldots,f_c^{H_\mathrm{f}},f_s^{H_\mathrm{f}},z_0,z_c^1,z_s^1,\ldots,z_c^{H_\mathrm{f}},z_s^{H_\mathrm{f}})^T \tag{23}$$

$\mathbf{L}(\,\cdot\,)$ is a linear operator and $\mathbf{Q}(\,\cdot\,,\cdot\,)$ is a quadratic operator. The expressions of $\mathbf{L}(\,\cdot\,)$ and $\mathbf{Q}(\,\cdot\,,\cdot\,)$ are not given here.

3.2.2. ANM step

The solutions of the quadratic algebraic system (21) with $N_\mathrm{eq}=2(2H+1)+2(2H_\mathrm{f}+1)+3$ equations and $N_\mathrm{eq}+1$ unknowns are made of one or several continuous branches. They can be computed with the ANM continuation method.

One of the main particularities of the ANM is that it gives access to branches of solutions in the form of power series. Assuming that we know a regular solution point U_0, the branch of solution passing through this point is computed in the form of a power series expansion (truncated at order N) of the pseudo-arclength path parameter $a=(U-U_0)^TU_1$, where U_1 is the tangent vector at U_0:

$$\mathbf{U}(a)=\mathbf{U}_0+\mathbf{U}_1a^1+\cdots+\mathbf{U}_Na^N \tag{24}$$

The series (24) is substituted into Eq. (21) and each power of a is equated to zero, giving a series of linear systems (involving the Jacobian matrix of $\mathbf{R}$ evaluated at U_0) characterizing the $\mathbf{U}_p(p\in[1,\ldots,N])$ [6].

The range of utility of the truncated power series (24) is limited because the series have a finite radius of convergence. Once each $\mathbf{U}_p$ ($p\in[0,\ldots,N]$) has been found, the range of utility a_max of the series expansion (24), satisfying

$$\|\mathbf{R}(a)\|<\varepsilon_\mathrm{tol},\quad \forall a\in[0,a_\mathrm{max}] \tag{25}$$

where ε_tol is a user-defined tolerance parameter, can be estimated [4].

The series (24) defines for $a\in[0,a_\mathrm{max}]$ a section of a branch of solution. A new section of a branch can be computed restarting the whole series calculation from $\mathbf{U}_0=\mathbf{U}(a_\mathrm{max})$.

One of the advantages of the ANM continuation approach is that the series (24) contain many useful information which can be advantageously used to define robust tools to detect bifurcation points [4] or to define indicator to locate and compute very efficiently any simple bifurcation point [5].

Finally, the ANM method needs a starting point. In our case, a periodic orbit of the underlying linear system can be used as a first point (one orbit) for initiating continuation.

The reader is referred to [4–6], for the details concerning the principle and the implementation of the ANM in the classical quadratic framework.

The MANLAB interactive package [20], which supports the proposed ANM continuation algorithm including bifurcation detection and branch switching, has been used to solve this quadratic algebraic system. Note that to reduce the numerical cost of the ANM, Fast Fourier Transform (FFT) algorithm has been implemented to compute efficiently the quadratic term $\mathbf{Q}(\mathbf{U},\mathbf{U})$ with a passage in the time domain as in the Alternating Frequency-Time HBM method.

3.3. Stability analysis

The linear stability of the NNM motions is characterized using Floquet theory [11].

Rewriting Eq. (10) into a first-order dynamical system, the stability of a periodic solution $\mathbf{p}_0(\tau)=[x_0(\tau)\ y_0(\tau)\ u_0(\tau)\ v_0(\tau)]$ of period T can be deduced from the eigenvalues of the monodromy matrix (also named the Floquet multipliers) associated with the fundamental matrix solution of the T-periodic variational linear differential system

$$\dot{\pi}(\tau)=\begin{pmatrix} 0 & 1 & 0 & 0 \\ -(1+\beta)+\dfrac{\partial f}{\partial x}(x_0(\tau);\alpha,\eta) & 0 & \beta & 0 \\ 0 & 0 & 0 & 1 \\ 0 & 0 & -\dfrac{\beta}{\delta} & \dfrac{\beta}{\delta} \end{pmatrix}\pi(\tau) \tag{26}$$

where an analytic expression of the gradient function $(\partial f/\partial x)(x;\alpha,\eta)$ is deduced from the implicit equation (8)) as

$$\frac{\partial f}{\partial x}(x;\alpha,\eta)=\frac{2\alpha^2(f(x;\alpha,\eta)^2-x(\tau)f(x;\alpha,\eta))-\alpha^2(x(\tau)^2-1)-\eta\alpha^2}{3f(x;\alpha,\eta)^2-4\alpha x(\tau)f(x;\alpha,\eta)}. \tag{27}$$

The monodromy matrix is computed over one period, using the four canonical basis vectors as initial conditions successively.

The autonomous equations of motion equation (10) defining an Hamiltonian system, it can be shown [10] that two Floquet multipliers are equal to one and the other two are reciprocal and complex-conjugate.

Hence, no Floquet multiplier can leave the unit circle with a nonzero imaginary part and the motion will be unstable only if at least one Floquet multiplier is greater than one or smaller than minus one.

4. Application

This section is dedicated to the analysis of the NNM of Eqs. (12)–(15) with the following numerical values: $\beta=1$, $\delta=1$ and $\alpha=30$ using the HBM–ANM method (η, H and H_{f} will be given later).

4.1. About the associated linear systems

To enlighten the behavior of the NNMs, it is useful to introduce a notation for the Linear Normal Modes (LNMs) of the various linear systems which are connected to the nonlinear system.

Three linear systems have been yet introduced: Eq. (5) which characterizes motions without impact and Eq. (6) (respectively Eq. (7)) which characterizes motions during the impact on the right (respectively left) elastic stop. One more linear system has to be considered. It is defined as

$$\begin{cases} \ddot{x}(\tau)+(1+\eta)x(\tau)+\beta(x(\tau)-u(\tau))=0 \\ \delta\ddot{u}(\tau)+\beta(u(\tau)-x(\tau))=0 \end{cases} \tag{28}$$

and corresponds to the underlying linear system around the equilibrium position associated to Eq. (10) (the regularized piecewise linear system).

These linear systems (Eqs. (5), (28), (6) and (7)) differ by the stiffness associated to the component x which is equal to 1, $1+\eta$, $1+\alpha$ and $1+\alpha$ respectively. In the sequel, the LNMs of the linear systems (Eqs. (5), (28) and (6)) will be denoted L_p^0, L_p^η and L_p^α respectively where the integer index p refers to the first ($p=1$) and second ($p=2$) linear normal mode. Note that the LNMs of Eq. (7) coincide with the LNMs of Eq. (6) and hence no distinction will made.

Finally, the last linear system considered in the sequel is the one with the mass at rest, $x(\tau)=0$. It is a 1-DOF system and the associated LNM will be denoted L_1^∞.

4.2. Validation of the HBM–ANM method

The objective here is to compare the NNMs of the piecewise linear system equations (3) and (4) obtained from the direct computation (see Section 2.2) and from the HBM–ANM method (Section 3.2) applied to Eqs. (12)–(15).

We focus on the first NNM starting at low energy level from the LNM L_1^0 (corresponding to the resonance frequency $\omega^2_{L_1^0}=(3-\sqrt{5})/2\approx 2\pi 0.098$). The starting point used in the HBM–ANM method is defined from the LNM L_1^η.

To implement the HBM–ANM method, the regularization parameter η and the harmonic numbers H and H_f have to be chosen. At low energy level, the NNM being approximated by the LNM L_1^η (corresponding to the resonance frequency $\omega_{L_1^\eta}^2 = (3+\eta-\sqrt{5+2\eta+\eta^2})/2$), the numerical value of η can be chosen such that $(|\omega_{L_1^0} - \omega_{L_1^\eta}|)/\omega_{L_1^0} < \epsilon_{\text{rel}}$. The results discussed here after have been obtained with $\eta = 0.005$ corresponding to the relative error $\epsilon_{\text{rel}} = 2 \times 10^{-3}$. The following numerical values will be used for the harmonic numbers: $H = 33$ and $H_f = 151$.

The NNMs obtained from the two approaches are compared in Fig. 4 in terms of Frequency-Energy Plot (FEP). The energy range considered here corresponds to periodic orbits with zero or one impact on each stop per period (see Section 2.2). As expected, the curves differ at low energy level due to the bias introduced by the parameter η. At high energy level, the curves coincide showing that $H = 33$, $H_f = 151$ is enough to correctly approximate the periodic orbits. However around the threshold energy level ($\approx 7 \times 10^{-1}$) where impacts occur, the approximation is less accurate due to the regularization procedure of the HBM–ANM method.

The period orbits obtained from the two approaches are compared in Fig. 5 for an intermediate energy level near the impact threshold energy level (point a in Fig. 4) and for a high energy level (point b in Fig. 4). At the first energy level (point a), the orbits obtained from the direct computation and from the HBM–ANM method slightly differ. The direct computation shows impacts (see Fig. 5, left) whereas the HBM–ANM method predicts x displacement in the range $]-1, 1[$ (no impact). However, in the configuration space, the modal curves are in very good agreement. At the second energy level (point b), the two approaches give results in very good agreement.

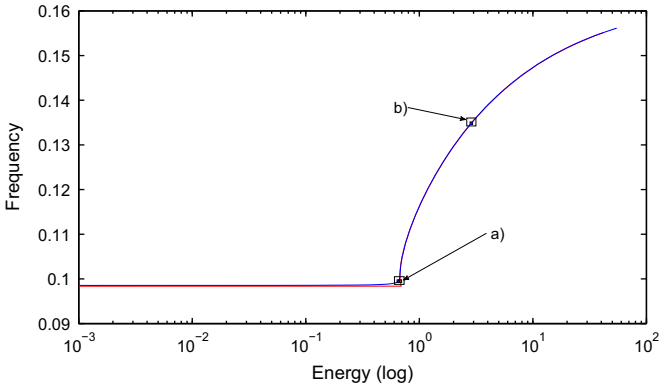

Fig. 4. FEP corresponding to the first NNM of the non-smooth system obtained from direct computation (in red) and from the HBM–ANM method (in blue). (Parameter values: $\alpha = 30$, $\beta = 1$, $\delta = 1$, $\eta = 0.005$, $H = 33$ and $H_f = 151$.) (For interpretation of the references to color in this figure caption, the reader is referred to the web version of this paper.)

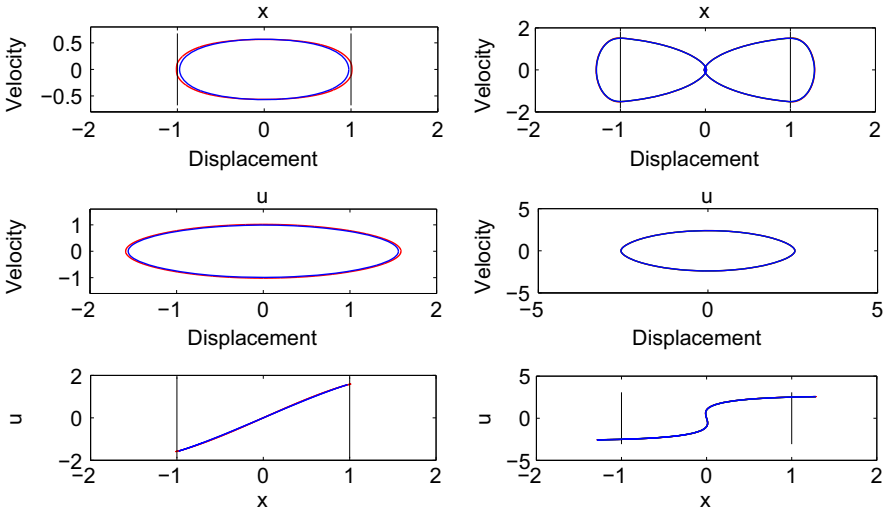

Fig. 5. Periodic orbits for points (a) and (b) in Fig. 4 obtained from direct computation (in red) and from the HBM–ANM method (in blue). First row: phase subspace $(x, \dot{x})$, second row: phase subspace $(u, \dot{u})$, third row: configuration space (x,u). (Parameter values: $\alpha = 30$, $\beta = 1$, $\delta = 1$, $\eta = 0.005$, $H = 33$ and $H_f = 151$.) (For interpretation of the references to color in this figure caption, the reader is referred to the web version of this paper.)

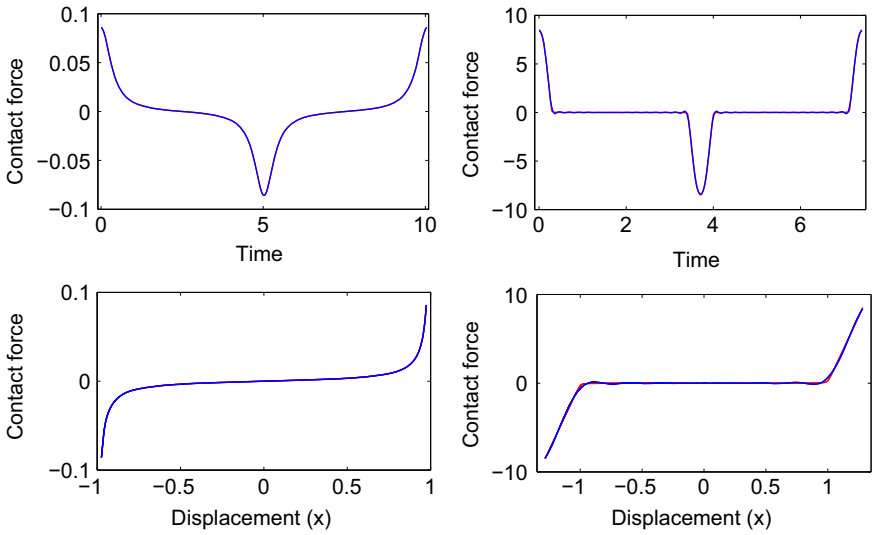

Fig. 6. Contact force for points (a) and (b) in Fig. 4 given by Eq. (9) (in red) and obtained from the HBM–ANM method (in blue). First row: time evolution over one period, second row: $(x, f(x))$-plot. (Parameter values: $\alpha=30$, $\beta=1$, $\delta=1$, $\eta=0.005$, $H=33$ and $H_f=151$.) (For interpretation of the references to color in this figure caption, the reader is referred to the web version of this paper.)

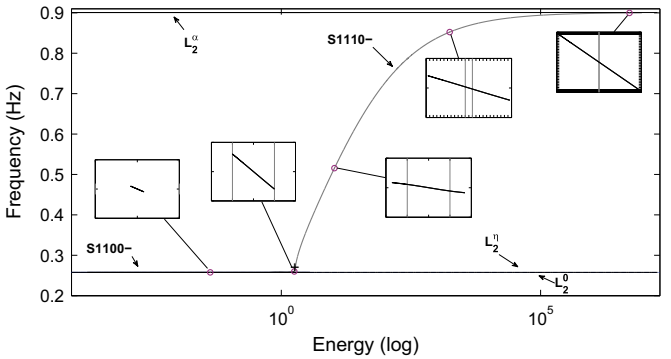

Fig. 7. FEP of the out-phase NNM. The black plus marker indicates the change of branches. (Parameter values: $\alpha=30$, $\beta=1$, $\delta=1$, $\eta=0.005$, $H=33$, $H_f=151$.)

The time series of the contact forces are shown in Fig. 6. In both cases (point a) and (point b), the two approaches give results in very good agreement.

These results show that the smoothness can be explicitly controlled and give a good approximation.

4.3. *Analysis of two NNMs of the regularized piecewise linear system*

The HBM–ANM method is now used to analyze in detail and on a large energy range two NNMs of the regularized piecewise linear system of equations (12)–(15), one starting from the LNM L_1^0 (the in-phase NNM) and the other starting from L_2^0 (the out-of-phase NNM). The following parameter values have been used: $\eta=0.005$, $H=33$ and $H_f=151$ to implement the HBM–ANM method. We checked that the curves were only very slightly modified by increasing H from 33 to 35.

As in [18,19], the following classification of the periodic orbits will be used:

(i) S*nmpq* $\pm$ denotes symmetric orbits with n and m the number of half waves in a half period respectively for the variable x and u. The indices p and q correspond respectively to the number of impacts for the first and second quarter period. The sign $\pm$ indicates if the curve in the configuration space (x,u) pass through the origin with positive or negative slope.
(ii) U*nmpq* denotes unsymmetric orbits with the same meaning for the integer indices than the previous one. Besides, there is no $\pm$ to indicate the sign of the slope because the motion is asynchronous and is represented by Lissajous curves in the configuration space (x,u).

4.3.1. The out-of-phase NNM

The out-of-phase NNM of the regularized piecewise linear system of Eqs. (12)–(15) is defined at low energy level by the LNM L_2^0 where the components of the associated mode shape have opposite sign. The behavior of the out-of-phase NNM is shown in Fig. 7 in terms of Frequency-Energy Plot (FEP). Modal line of periodic orbits is also reported in Fig. 7 in the configuration space (x,u). The tick mark locations are given at the multiples of the gap 1 in x and u direction and two vertical lines represent the gap positions in x direction. At low energy level, the branch starts with S1100− motions (black branch) and it coincides with the LNM L_2^η which is close to LNM L_2^0. At the impact threshold energy level, S1110− motions (one impact per half period) take place and this type of motions persists when the energy level increases (dark gray branch) up to the LNM L_2^α.

4.3.2. The in-phase NNM

The in-phase NNM of the regularized piecewise linear system of Eqs. (12)–(15) is defined at low energy level by the LNM L_1^0 where the components of the associated mode shape have the same sign. The behavior of the in-phase NNM is shown in Fig. 8(a) in terms of FEP with close ups in Fig. 8(b) and (c). Similar to the out-of-phase NNM, the branch starts, at low energy level, with S1100+ motions (black branch) and it coincides with the LNM L_1^η which is close to LNM L_1^0 (see Fig. 8(a)). At very hight energy level, S1110+ motions take place and this type of motions persists when the energy level increases (dark gray branch) up to the LNM L_1^α (see Fig. 8(a)). Moreover and contrary to the out-of-phase NNM, more complicated dynamics are

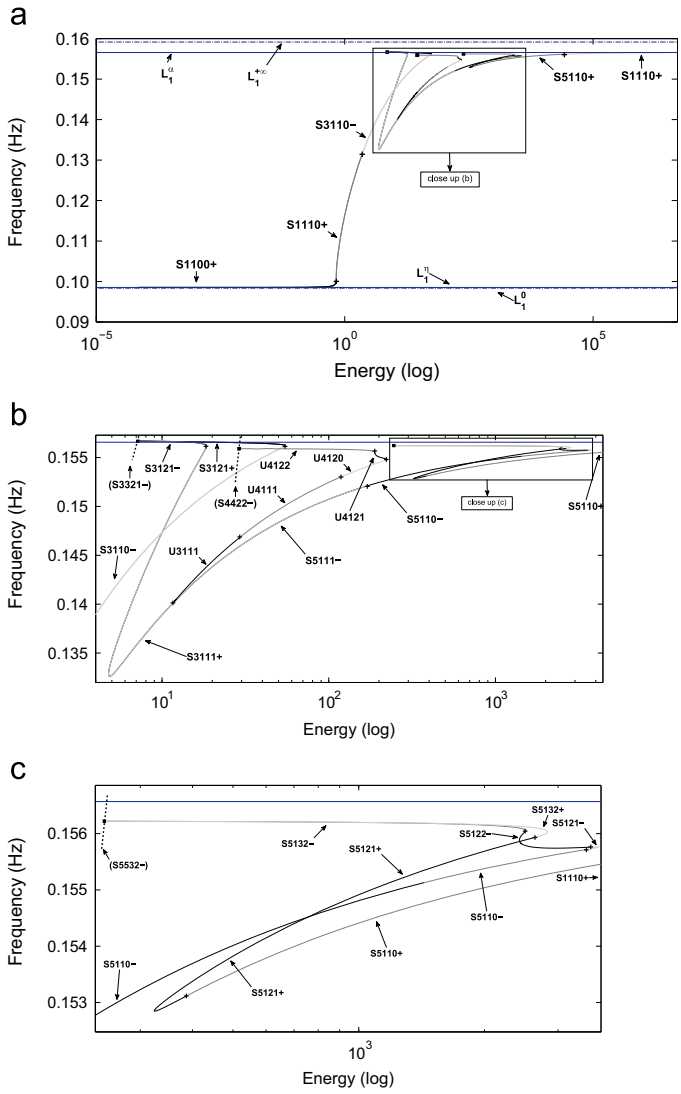

Fig. 8. FEP of the in-phase NNM: (a) overview, (b) and (c) close ups. The black square markers indicate internal resonances. The black plus markers indicate the change of branches. (Parameter values: $\alpha=30$, $\beta=1$, $\delta=1$, $\eta=0.005$, $H=33$, $H_f=151$.)

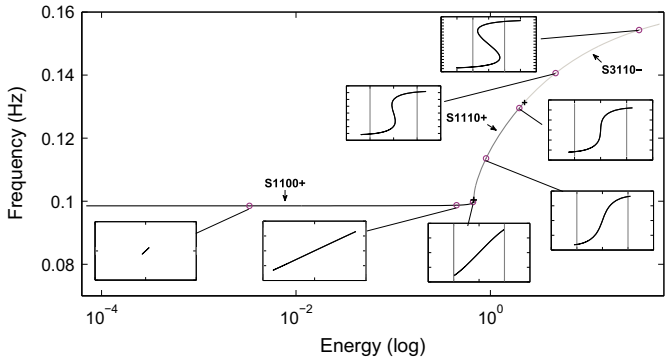

Fig. 9. Zoom on particular branches (S1100+, S1110+, S3110−) of the FEP of the in-phase NNM, some periodic orbits are represented by modal line (see the boxes). The black plus markers indicate the change of branches. (Parameter values: $\alpha=30$, $\beta=1$, $\delta=1$, $\eta=0.005$, $H=33$, $H_f=151$.)

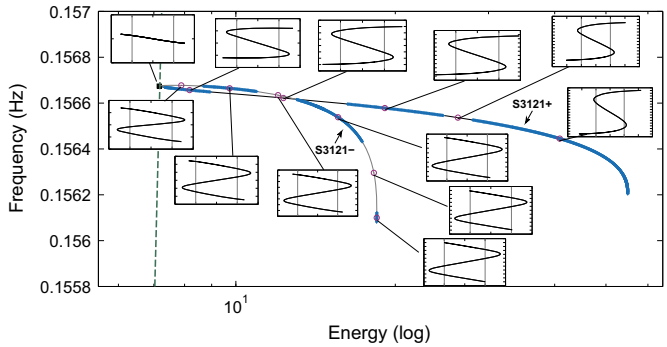

Fig. 10. Zoom on particular branches (S3121−, S3121+) of the FEP of the in-phase NNM, some periodic orbits are represented by modal line (see the boxes). The instability is depicted by dark blue (+) (Floquet multiplier greater than +1). The black square marker indicates the internal resonance. (Parameter values: $\alpha=30$, $\beta=1$, $\delta=1$, $\eta=0.005$, $H=33$, $H_f=151$.) (For interpretation of the references to color in this figure caption, the reader is referred to the web version of this paper.)

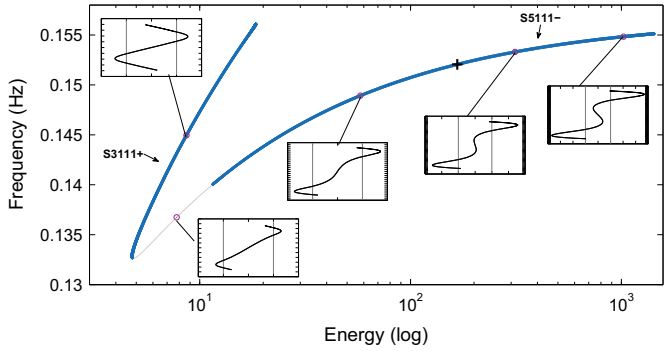

Fig. 11. Zoom on particular branches (S3111+, S5111−) of the FEP of the in-phase NNM, some periodic orbits are represented by modal line (see the boxes). The instability is depicted by dark blue (+) (Floquet multiplier greater than +1). The black plus marker indicates the change of branches. (Parameter values: $\alpha=30$, $\beta=1$, $\delta=1$, $\eta=0.005$, $H=33$, $H_f=151$.) (For interpretation of the references to color in this figure caption, the reader is referred to the web version of this paper.)

observed between these two states (see the close ups in Fig. 8(b) and (c)) characterized by period motions with the number of impacts which increases and internal resonances. Three internal resonances have been identified. They emanate from interaction of the in-phase NNM with the out-of-phase NNM. The first internal resonance is associated to the tongue (S3121+, S3121−) (see Fig. 8(b)) and corresponds to a 3:1 internal resonance between the in-phase and out-of-phase NNMs. The second internal resonance is associated to the tongue (U4122) (see Fig. 8(b)) and corresponds to a 4:1 internal resonance and the last one is associated to the tongue (S5132+, S5132−) (see Fig. 8(c)) and corresponds to a 5:1 internal resonance.

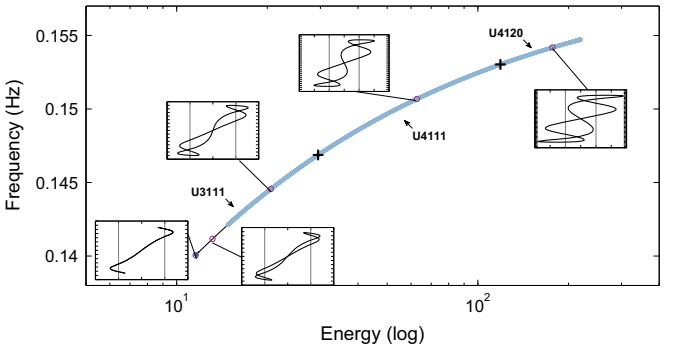

Fig. 12. Zoom on particular branches (U3111, U4111, U4120) of the FEP of the in-phase NNM, some periodic orbits are represented by modal line (see the boxes). The instability is depicted by light blue (o) (Floquet multiplier smaller than -1). The black plus markers indicate the change of branches. (Parameter values: α=30, β=1, δ=1, η=0.005, H=33, $H_f = 151$.) (For interpretation of the references to color in this figure caption, the reader is referred to the web version of this paper.)

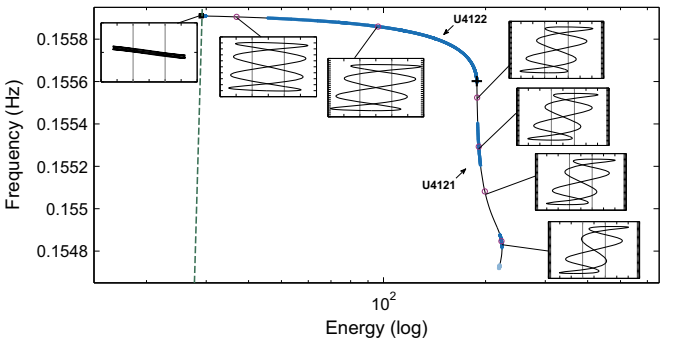

Fig. 13. Zoom on particular branches (U4122, U4121) of the FEP of the in-phase NNM, some periodic orbits are represented by modal line (see the boxes). The instability is depicted by dark blue ($+$) when a Floquet multiplier is greater than $+1$, and by light blue ($\circ$) when a Floquet multiplier is smaller than -1. The black plus marker indicates the change of branches. The black square marker indicates the internal resonance. (Parameter values: α=30, β=1, δ=1, η=0.005, H=33, $H_f = 151$.) (For interpretation of the references to color in this figure caption, the reader is referred to the web version of this paper.)

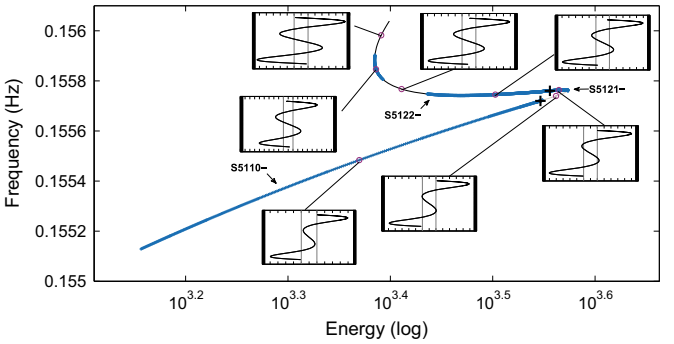

Fig. 14. Zoom on particular branches (S5110 −, S5121 −, S5122 −) of the FEP of the in-phase NNM, some periodic orbits are represented by modal line (see the boxes). The instability is depicted by dark blue ($+$) (Floquet multiplier greater than $+1$). The black plus markers indicate the change of branches. (Parameter values: α=30, β=1, δ=1, η=0.005, H=33, $H_f = 151$.) (For interpretation of the references to color in this figure caption, the reader is referred to the web version of this paper.)

It is interesting to note the absence of the internal resonance 2:1 which is due to asymmetrical spring configuration of the model (see for example the system [25]), and also the absence of internal resonances k:1 for $k > 5$ which is due to the stiffness parameter α of the system (see Section 4.3.3).

To understand the behavior of this complicate NNM, zooms on different branches of FEP are analyzed in detail in Figs. 9 and 16 reporting some representative periodic orbits in the configuration space (x,u) and including stability properties.

Fig. 9 shows the branches S1100+ (black curve), S1110+ (dark gray curve), S3110− (light gray curve). All the branches characterize stable periodic motions. As already mentioned, the branch S1100+ coincides with the LNM L_1^η which ends

when the energy (or the amplitude) is sufficient for the first mass (x component) to reach the stop. From this point modal straight lines in the configuration space are replaced by modal curved lines. Then the amplitude of the second mass (u component) increases whereas that the amplitude of the first mass which is limited by the elastic stop. This behavior implies a change of the sign of the slope of the modal line (on the neighborhood of the origin), and the apparition of a new oscillation. The transition between S1110+ and S3110− occurs. This new oscillation increases with the energy level and the first mass (x component) reaches the stops. A new impact occurs which corresponds to the transition between S3110− and S3121−.

Fig. 10 shows the branches S3121− (dark gray curve), S3121+ (light gray curve) corresponding to the first tongue. Following the branch S3121−, the energy level decreases and only the amplitude of the second mass is mainly influenced. This type of motions persists up to the modal curved lines tend towards a modal straight line where a bifurcation point between the in-phase NNM and the branch S1110− of the out-of-phase NNM (depicted on three-period given a S3121− motion corresponding to dashed line named (S3121−) in Fig. 10) is reached (see black square) defining an internal resonance 3:1. At this point, the transition between S3121− and S3121+ also occurs with the change of sign of the slop of the modal line. Increasing the energy level, the S3121+ branch vanishes when the number of impacts decreases and the transition between S3121+ and S3111+ occurs. Note that instability zones have been detected on these branches.

Fig. 11 shows the branches S3111+ and S5111−. The transition between S3111+ and S5111− occurs at the black (+). This point corresponds to the increase in the oscillation of the x motion. Another important phenomenon is the appearance of a bifurcation point (see black circle), obtained by the method described in [5]. This bifurcation point does not correspond to an internal resonance but leads to a new branch of periodic solutions. This secondary branch is the tongue associated to the even internal resonance 4:1 (see Figs. 12 and 13).

Fig. 12 (respectively Fig. 13) shows the branches U3111, U4111, U4120 (respectively U4121, U4122). The motions here are no more symmetric, however some kinds of phenomenon such as variations of the number of oscillations and variations of the number of impacts are observed, but only for a half-period. After the transition between U4121 and U4121 (see black (+) Fig. 13) the motions persist up to the modal curved lines tend towards a modal line where a bifurcation point between the in-phase NNM and the branch S1110− of the out-of-phase NNM (depicted on four-period given a S4422− motion corresponding to dashed line named (S4422−) in Fig. 13) is reached (see black square) defining the internal resonance 4:1. We can also observed that for these branches instabilities occur (with a Floquet multiplier greater than +1).

Fig. 14 shows the branches S5110−, S5121−, S5122− on the main backbone of the FEP. These branches correspond to symmetric motions. Oscillations occur during the first and the second half-period, and the first mass (x component) reaches the elastic stop increasing the number of impacts (transition between S5110−, and S5121− and between S5121− and S5122−) without changing the number of half waves. Hence internal resonance cannot occur here. The number of impacts needs to be equal to five, which happens at the end of the branch S5122−.

Fig. 15 shows the part of the third tongue where the internal resonance 5:1 occurs (branches S5132− and S5132+). These two branches (in the FEP plot) are nearly identical and they are plotted separately. As observed for the 3:1 internal resonance, a bifurcation point between the in-phase NNM and the branch S1110− of the out-of-phase NNM (depicted on five-period given a S5132− motion) is reached. At this point, the transition between S5132− and S5132+ also occurs with the change of sign of the slop of the modal line.

Finally the last part of the main backbone of the FEP is shown Fig. 16. The same phenomenon observed on the branch S3111+ is observed here, so the number of impacts decreases. But instead of the apparition of an oscillation when the energy starts to increase, which implies new impacts, the amplitude of the second mass increases and the impacts disappear. The period motions are now close to the LNM L_1^a.

It is interesting to note that the frequency contains of the backbone of the in-phase NNM can be greater than $\omega_{L_1^a}$ (see Fig. 10). An upper bound is given by $\omega_{L_1^\infty}$ (see Fig. 8).

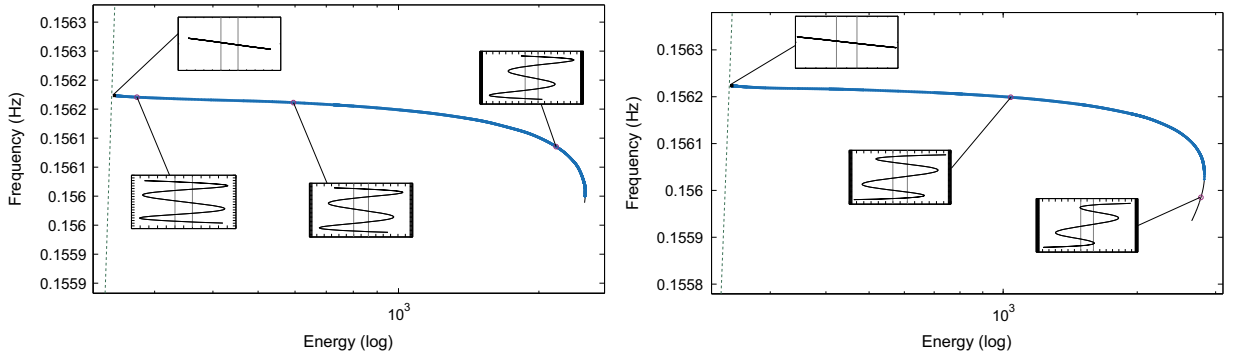

Fig. 15. Zoom on particular branches (S5132− at left, S5132+ at right) of the FEP of the in-phase NNM, some periodic orbits are represented by modal line (see the boxes). The instability is depicted by dark blue (+) (Floquet multiplier greater than +1). The black square marker indicates the internal resonance. (Parameter values: $\alpha=30$, $\beta=1$, $\delta=1$, $\eta=0.005$, $H=33$, $H_t=151$.) (For interpretation of the references to color in this figure caption, the reader is referred to the web version of this paper.)

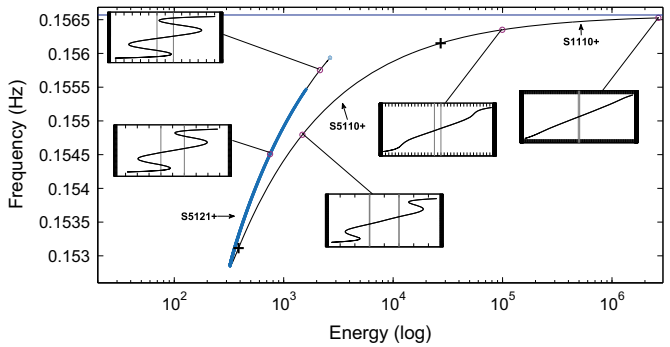

Fig. 16. Zoom on particular branches (S5121+, S5110+, S1110+) of the FEP of the in-phase NNM, some periodic orbits are represented by modal line (see the boxes). The instability is depicted by dark blue (+) (Floquet multiplier greater than +1). The black plus markers indicate the change of branches. (Parameter values: $\alpha=30$, $\beta=1$, $\delta=1$, $\eta=0.005$, $H=33$, $H_f=151$.) (For interpretation of the references to color in this figure caption, the reader is referred to the web version of this paper.)

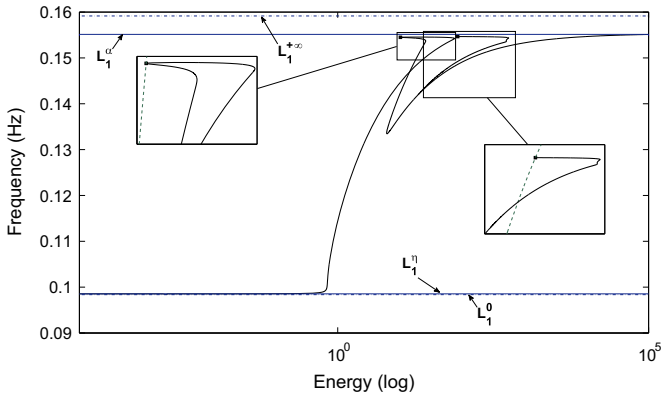

Fig. 17. FEP of the first NNM, with $\alpha=20$. (Parameter values: $\beta=1$, $\delta=1$, $\eta=0.005$, $H=33$, $H_f=151$.)

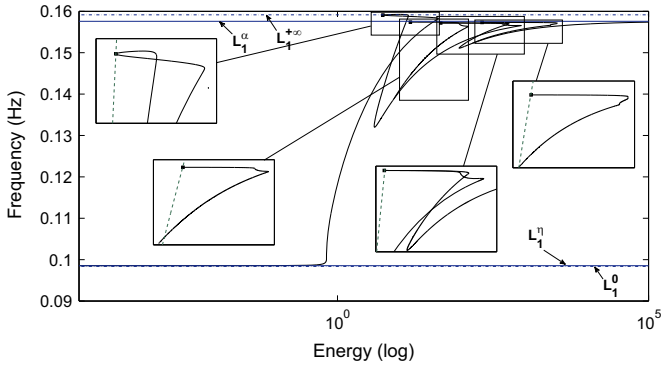

Fig. 18. FEP of the first NNM, with $\alpha=50$. (Parameter values: $\beta=1$, $\delta=1$, $\eta=0.005$, $H=33$, $H_f=201$.)

4.3.3. About the parameter α

The objective of this section is to evaluate the influence of the parameter α on the dynamics richness of the in-phase NNM.

Figs. 17 and 18 show the behavior of the in-phase NNM in terms of FEP for $\alpha=20$ and $\alpha=50$.

We note that we use for $\alpha=50$ a higher number of harmonics $H_f=201$ to have a better precision.

We observe that the parameter α (stiffness of the elastic stop) influences the number of internal resonance. For $\alpha=20$, we have only the internal resonances 3:1 and 4:1 whereas for $\alpha=50$ we have the internal resonances 3:1, 4:1, 5:1 and 6:1.

Note that the odd internal resonances appear as the turning points of the main branch whereas the even internal resonances appear as a turning point of the secondary branches.

As already mentioned, the upper bound in terms of frequency of the backbone of the in-phase NNM is given by $\omega_{L_1^\infty}$. By increasing α the asymptotic limit $\omega_{L_1^\alpha}$ increases and tends to approach the limit $\omega_{L_1^\infty}$. The comparison of Figs. 17, 8 and 18 helps to understand this phenomenon that is the increase of the number of internal resonance with α.

5. Conclusion

The computation of the nonlinear normal modes of a two degrees-of-freedom with a piecewise linearity was performed using a numerical procedure, called regularization-HBM–ANM. This procedure combines a regularization of the contact force, the harmonic balance method and the asymptotic numerical method. The HBM was considered using Fourier series with different order of truncation for linear and nonlinear components. Moreover, stability analysis of the periodic orbits was carry out using Floquet theory, reminding also the specificity of 2-DOF Hamiltonian system. The regularization-HBM–ANM method was validated comparing the results with a direct computation of the periodic solutions of the piecewise linear system when only two impact per period occur. Some particular behavior was observed more often for the in-phase nonlinear normal mode. The first was the absence of the internal resonance 2:1 due to the asymmetrical spring configuration. Moreover, the stiffness of the spring of the elastic stop influences the number of internal resonance. The NNMs tend asymptotically to the in-phase linear normal mode of the system where the spring of the elastic stop is directly connected to the mass (in other words for a gap equal to zero). Besides, the odd internal resonances appear as the turning points of the main branch whereas the even internal resonances appear as a turning point of the secondary branches. These efficient numerical procedures can be used to compute NNMs of industrial structure.

References

[1] U. Andeaus, P. Casini, F. Vestroni, Non-linear dynamics of a cracked cantilever beam under harmonic excitation, Int. J. Non-linear Mech. 42 (2007) 566–575.
[2] R. Arquier, S. Bellizzi, R. Bouc, B. Cochelin, Two methods for the computation of nonlinear modes of vibrating systems at large amplitudes, Comput. Struct. 84 (2006) 1565–1576.
[3] S. Chen, S. Shaw, Normal modes for piecewise linear vibratory systems, Nonlinear Dyn. 10 (1996) 135–164.
[4] B. Cochelin, N. Damil, E. Allgowe, Méthode asymptotique numèrique, Hermes Lavoisier, Paris, 2007.
[5] B. Cochelin, M. Medale, Power series analysis as a major breakthrough to improve the efficiency of asymptotic numerical method in the vicinity of bifurcations, J. Comput. Phys. 236 (2012) 594–607.
[6] B. Cochelin, C. Vergez, A high order purely frequency-based harmonic balance formulation for continuation of periodic solutions, J. Sound Vib. 324 (1–2) (2009) 243–262.
[7] N. Coudeyras, S. Nacivet, J.-J. Sinou, Periodic and quasi-periodic solutions for multi-instabilities involved in brake squeal, J. Sound Vib. 328 (2009) 520–540.
[8] E.K. Ervin, J.A. Wickertb, Repetitive impact response of a beam structure subjected to harmonic base excitation, J. Sound Vib. 307 (2000) 2–19.
[9] A. Grolet, F. Thouverez, On a new harmonic selection technique for harmonic balance method, Mech. Syst. Signal Process. 30 (2012) 43–60.
[10] J.D. Hadjedemetriou, Periodic orbits in gravitational systems, in: B. Steves, A. Maciejewski, M. Hendry (Eds.), Chaotic Worlds: From Order to Disorder in Gravitational N-Body Dynamical Systems, 2006, pp. 43–79.
[11] J. Hale, Ordinary Differential Equations, Wiley-Interscience, New York, 1969.
[12] V. Jaumouillé, J.-J. Sinou, B. Petitjean, An adaptive harmonic balance method for predicting the nonlinear dynamic responses of mechanical systems—application to bolted structures, J. Sound Vib. 329 (19) (2010) 4048–4067.
[13] D. Jiang, C. Pierre, S.W. Shaw, Large-amplitude non-linear normal modes of piecewise linear systems, J. Sound Vib. 272 (2004) 869–891.
[14] S. Karkar, B. Cochelin, C. Vergez, A high-order, purely frequency based harmonic balance formulation for continuation of periodic solutions: the case of non-polynomial nonlinearities, J. Sound Vib. 332 (2013) 968–977.
[15] G. Kerschen, M. Peeters, J. Golinval, A. Vakakis, Nonlinear normal modes, part i: a useful framework for the structural dynamicist, Mech. Syst. Signal Process. 23 (2009) 170–194.
[16] C. Lamarque, O. Janin, Modal analysis of mechanical systems with impact non-linearities: limitations to a modal superposition, J. Sound Vib. 235 (4) (2000) 567–609.
[17] D. Laxalde, F. Thouverez, Complex non-linear modal analysis for mechanical systems: application to turbomachinery bladings with friction interfaces, J. Sound Vib. 322 (2009) 1009–1025.
[18] Y.S. Lee, G. Kerschen, A.P.P. Vakakis, L.A. Bergmand, D.M. McFarland, Complicated dynamics of a linear oscillator with a light, essentially nonlinear attachment, Physica D 204 (2005) 41–69.
[19] Y.S. Lee, F. Nucera, A. Vakakis, D.M. McFarland, L.A. Bergmand, Periodic orbits, damped transitions and targeted energy transfers in oscillators with vibro-impact attachments, Physica D 238 (2009) 1868–1896.
[20] MANLAB, An interactive path-following and bifurcation analysis software. http://manlab.lma.cnrs-mrs.fr, 2012.
[21] Y. Mikhlin, A. Vakakis, G. Salenger, Direct and inverse problems encountered in vibro-impact oscillations of a discrete system, J. Sound Vib. 216 (2) (1998) 227–250.
[22] A. Nayfeh, B. Balachandran, Applied Nonlinear Dynamics: Analytical, Computational and Experimental Methods, John Wiley, New York, 1995.
[23] M. Pascal, Dynamics and stability of a two degree of freedom oscillator with an elastic stop, J. Comput. Nonlinear Dyn. 1 (2006) 94–102.
[24] M. Peeters, G. Kerschen, J. Golinval, Modal testing of nonlinear vibrating structures based on nonlinear normal modes: experimental demonstration, Mech. Syst. Signal Process. 25 (2011) 1227–1247.
[25] M. Peeters, R. Viguié, G. Sérandour, G. Kerschen, J.-C. Golinval, Nonlinear normal modes, part ii: toward a practical computation using numerical continuation techniques, Mech. Syst. Signal Process. 23 (2009) 195–216.
[26] V. Pilipchuk, A. Vakakis, M. Azeez, Study of a class of subharmonic motions using a non-smooth temporal transformation (nstt), Physica D 100 (1997) 145–164.
[27] R. Rosenberg, On nonlinear vibrations of systems with many degree of freedom, Adv. Appl. Mech. 242 (9) (1966) 155–242.
[28] R. Seydel, Practical Bifurcation and Stability Analysis, From Equilibrium to Chaos, Springer-Verlag, New York, 1994.
[29] S. Shaw, P. Holmes, A periodically forced piecewise linear oscillator, J. Sound Vib. 90 (1983) 129–155.
[30] S. Shaw, C. Pierre, Non-linear normal modes and invariant manifolds, J. Sound Vib. 150 (1) (1991) 170–173.
[31] C. Toulemonde, C. Gontier, Sticking motions of impact oscillators, Eur. J. Mech., A/Solids 17 (2) (1988) 339–366.

[32] A. Vakakis, Non-linear normal modes (nnms) and their applications in vibration theory: an overview, Mech. Syst. Signal Process. 11 (1) (1997) 3–22.
[33] A. Vakakis, O. Gendelman, L. Bergman, D. McFarland, G. Kerschen, Y. Lee, Nonlinear Targeted Energy Transfer in Mechanical and Structural Systems I & II, Springer, Netherlands, 2008.
[34] A. Vakakis, L. Manevitch, Y. Mikhlin, V. Pilipchuk, A. Zevin, Normal Modes and Localization in Nonlinear Systems, Wiley, New York, 1996.
[35] K. Woo, A.A. Rodger, R.D. Neilson, M. Wiercigroch, Application of the harmonic balance method to ground moling machines operating in periodic regimes, Chaos Solitons Fractals 11 (2000) 2515–2525.